Image Cover Sheet

CLASSIFICATION	SYSTEM NUMBER
UNCLASSIFIED	103732

TITLE

A REFINED MAXIMUM LIKELIHOOD METHOD FOR TRACKING LOW-ALTITUDE TARGETS OVER THE SEA: RESULTS OF SIMULATION AND EXPERIMENTS

System Number:

Patron Number:

Requester:

Notes:

DSIS Use only:

Deliver to:

National Defence / Défense nationale

A REFINED MAXIMUM LIKELIHOOD METHOD FOR TRACKING LOW-ALTITUDE TARGETS OVER THE SEA: RESULTS OF SIMULATION AND EXPERIMENTS (U)

by

Eloi Bossé, Ross M. Turner and Daniel Brookes

DEFENCE RESEARCH ESTABLISHMENT OTTAWA
REPORT NO. 1103

Canada

December 1991
Ottawa

National Defence / Défense nationale

A REFINED MAXIMUM LIKELIHOOD METHOD FOR TRACKING LOW-ALTITUDE TARGETS OVER THE SEA: RESULTS OF SIMULATION AND EXPERIMENTS (U)

by

Eloi Bossé, Ross M. Turner
Surface Radar Section
Radar Division

and

Daniel Brookes
Advanced Information Technologies (AIT)

DEFENCE RESEARCH ESTABLISHMENT OTTAWA
REPORT NO. 1103

PCN
011LA

December 1991
Ottawa

A Refined Maximum Likelihood Method for Tracking Low–Altitude Targets over the Sea: Results of Simulation and Experiments.

by

Éloi Bossé, Ross M. Turner, Daniel E. Brookes

Abstract

Accurate radar tracking of targets flying at low altitudes above a smooth surface is difficult because of the surface reflection. We propose a solution based on deterministic physical modelling of the specular multipath and the maximum likelihood method. This paper describes the techniques and the results of performance studies. We derive the Cramer–Rao bound and show the benefit of using the refined propagation model. Monte–Carlo simulations are employed to compare the performance with the Cramer–Rao bound and demonstrate threshold effects on target height estimation. Finally we present the results obtained with two X–band radar experimental systems.

RÉSUMÉ

Le pistage précis d'une cible radar volant au–dessus d'un plan d'eau est rendu difficile par la présence des réflections sur la surface. Nous proposons dans ce cas d'inclure un modèle spéculaire de la propagation multivoie. Ce modèle est utilisé avec le Maximum de Vraisemblance. Dans ce rapport nous présentons la technique, dérivons la limite de Cramer–Rao et présentons des résultats de simulation indiquant que l'emploi d'un modèle spéculaire améliore grandement la précision. Nous présentons finalement des résultats expérimentaux obtenus par deux systèmes radar opérant dans la bande X. Nous démontrons que l'utilisation d'un modèle spéculaire donne un bon pistage là où l'approche conventionelle ne fonctionne pas.

EXECUTIVE SUMMARY

This report presents a new method for low–angle radar tracking in the presence of specular multipath. We define new estimators based on the maximum likelihood criterion for estimating the height of targets flying at low altitudes over the sea. We assume that interfering multipath signals are present and show that identifying and modelling the nature of the multipath interference can have a beneficial effect on the estimation of desired parameters.

Previous experimental works indicated that at low altitude the interference pattern can be accurately predicted under normal propagation conditions. We use that information in an optimal way in the context of the maximum likelihood (ML) estimation theory and we name this algorithm the Refined Maximum Likelihood (RML) technique.

We use real multipath data to test the RML technique. In recent years, DREO (Defence Research Establishment Ottawa, Canada) has been undertaken many trials to collect real multipath data on the Ottawa River. As part of the ELAT (Experimental Low–Angle Tracking radar), an 8–element sampled aperture antenna was used to collect the data at two frequencies: 8.6 and 9.6 GHz. The target was a high–power beacon source. Also, in late October 1987, a series of experiments was performed on the west coast of the Bruce Peninsula overlooking Lake Huron (Canada). This time, the MARS (Multi–parameter Adaptive Radar System) developed at the Communications Research Laboratory (CRL), McMaster University (Canada) was used. MARS has a 32–element sampled aperture antenna which was used to collect data at multiple frequencies within the 8–12 GHz band. Here again, the target was simulated by a beacon source. Data collected by these two systems form our experimental data base to test our technique.

The results of simulations and experiments indicate substantial improvements with the RML algorithm compared with conventional techniques such as Fourier beamforming. The results show some robustness of the RML technique in the presence of diffuse multipath with experimental results obtained in sea state 3 conditions.

CONTENTS

A Refined Maximum Likelihood Method for Tracking Low–Altitude Targets over the Sea: Results of Simulation and Experiments.

1.0 INTRODUCTION

This paper presents a new method for low–angle tracking in the presence of specular multipath. We define new estimators based on the maximum likelihood criterion for estimating the height of targets flying at low altitudes over the sea. The problem investigated is direction finding for a single target in the presence of specular reflection from a relatively smooth flat surface such as the sea. In recent years a considerable amount of research has been done in the area of signal processing, using superresolution algorithms to separate a target from its image and to provide an accurate estimate of the target's elevation. Our approach is essentially different; we assume that interfering multipath signals are present and show that identifying and modelling the nature of the multipath interference can have a beneficial effect on the estimation of desired parameters.

Barton [1] summarizes the low–angle tracking work up to 1974. His paper presents a number of methods to combat multipath errors. Most of these methods use monopulse and they all fail to resolve targets separated by less than 0.25 beamwidth. More recently Haykin and Kesler [2,3] propose an adaptive canceller and Haykin [4] investigates the use of high resolution techniques such as autoregression, maximum entropy and linear prediction. It seems [5] that a limit of 0.25 beamwidth applies to most high resolution techniques [6], including the well known MUltiple SIgnal Classification (MUSIC) method [7]. MUSIC and most of these techniques fail to resolve correlated signals such as those encountered with multipath; here the direct ray is fully correlated with the reflected ray and the required resolution can be as high as than 0.05 beamwidth.

There are a number of more or less efficient techniques to decorrelate the signals. Pillai [8] discusses techniques using spatial smoothing. With this technique, we form sub–arrays and average the corresponding covariance matrices. Pillai shows that to detect the arrival angles for two closely spaced, equi–power, correlated signals, requires increasing the number of sample vectors (snapshots) by a factor of approximately $[(1/K\omega_d)^2 - 1]$ in

comparison with the number required for uncorrelated signals. Parameter K represents the number of sensors and $\omega_d = \pi(\cos\theta_1 - \cos\theta_2)/2$ is related to angular separation between signals. For low–angle tracking, we would require a considerably increased number of snapshots. The factor is larger than 10000 since the angular separation between the target direction θ_1 and the image direction θ_2 may be less than one degree. Other techniques [9,10] use a multidimensional search with multiple parameters, imposing a high computational burden that may be impractical for low–angle tracking.

We propose a different technique which incorporates a highly descriptive model of the physics of the low–angle problem. Previous experimental works [11–13] indicated that at low altitude the interference pattern can be accurately predicted under normal propagation conditions. Litva [14–16] first used a similar model in an algorithm called CHA (Correlation Height Analysis) and obtained resolution up to 1/28 of a beamwidth [16] under normal propagation conditions and smooth sea surface. We use the idea of a detailed propagation model but in the context of the maximum likelihood (ML) estimation theory and we name this algorithm the Refined Maximum Likelihood (RML) technique [17–19].

In this paper, we present the first development phase of the RML technique where the propagation model assumes a medium that is linear, homogeneous, isotropic and frequency invariant (narrow–band). The effects of anomalous propagation, ducting, sea roughness and sea swell are under investigation and results will be reported as a second paper. The RML technique is designed to work in situation where other high resolution methods fail to resolve the target from its image. If the angular separation between the target and its image is greater than one beamwidth, a monopulse or Fourier beamforming method can be used. This is simpler, more robust and computationally more efficient than the RML technique.

Maximum likelihood estimation has been applied to angle–of–arrival estimation using an angle–of–arrival (AOA) model. In [20], a comparative study of a number of apparently different angle estimation techniques [21–28] showed that they were, in fact, ML techniques using the AOA model.

The AOA model has an unknown angle and an unknown complex amplitude for each signal; specular multipath is represented by two such signals in the AOA model yielding six parameters which must be implicitly estimated. In contrast, we use a priori

information to reduce the number of unknowns in our propagation model; specular multipath is modelled with only three unknowns: an amplitude, a phase and the target height. To obtain the information required by the model, the radar is operated in an acquisition mode to determine target range and doppler velocity. Prior knowledge about the geometry and the specular reflection coefficient is assumed. This is not a very restrictive assumption for low–angle tracking because the reflection coefficient is almost -1 under smooth sea conditions. Sea roughness and divergence due to surface curvature are taken into account by decreasing the amplitude of the specular reflected ray. Using this model we have accurately tracked beacon targets over rough sea conditions (sea state 3).

We use real multipath data to test the RML technique. In recent years, DREO (Defence Research Establishment Ottawa, Canada) has been undertaken many trials to collect real multipath data on the Ottawa River. As part of the ELAT (Experimental Low–Angle Tracking radar), an 8–element sampled aperture antenna was used to collect the data. The target was a high–power beacon source. Also, in late October 1987, a series of experiment were performed on the west coast of the Bruce Peninsula overlooking Lake Huron (Canada). This time, the MARS (Multi–parameter Adaptive Radar System) developed at the Communications Research Laboratory (CRL), McMaster University (Canada) was used. MARS has a 32–element sampled aperture antenna which was used to collect data at multiple frequencies. Here again, the target was simulated by a CW beacon. Data collected by these two systems form our experimental data base to test our technique.

The paper is organized as follows. Section 2 presents the propagation model. In Section 3, we derive the RML height estimators. Section 4 contains the derivations of the Cramer–Rao bounds. Section 5 gives the results of simulations and Section 6 terminates with the experimental results. We use the following notation: matrices are represented by bold upper–case letters, vectors by bold lower–case letter, scalars by both upper and lower italic letters. The superscripts, $\hat{}$, $*$, ^{T}, ^{H}, $\| \ \|$ denote estimate, conjugation, transposition, conjugation–transposition, and vector norm respectively. Also $\mathbb{C}^{M*N}$ signifies a M×N complex matrix.

2 The Propagation model

The propagation model used in this paper assumes a medium that is linear, homogeneous, isotropic and frequency invariant (narrow–band). The model considers

bipath propagation with only a single reflected ray emanating from a virtual target image. We assume that the targets are located at such a distance from the receiving antenna that the impinging waves can be considered as being planar. We consider a two–way transmission model (radar model) and a one–way transmission model (beacon model). The beacon model is important for experimental investigations. It is much easier and less expensive to set up a beacon system and a receiving array with narrow–band receivers than to implement a radar system with its much more complicated transmission and reception system. The experimental results presented in this paper are obtained using a beacon as a target; experimental verification using a radar transmitter is ongoing.

The geometry for the beacon model is illustrated in Fig.1 assuming an equivalent flat–earth model with parameters compensated for the effects of the earth's curvature. The noise–free observation model for a signal received at the k$^{\text{th}}$ element of an array of K sensors is

$$v_k = Q_1 \, exp(-j\xi R) \, exp\{-j\xi(z_k^2 + h_k^2)/2R\} \times [exp(j\xi h_k z_k/R) + A \, exp(-j\xi h_k z_k/R)], \tag{2.1}$$

where $\xi = 2\pi/\lambda$, λ is the wavelength, z_k is the height of the k$^{\text{th}}$ element, R is the target range, h_k is the target height, and Q_1 is an unknown complex amplitude due to target characteristics. The complex amplitudes of the direct and reflected rays are simply related by a complex multipath reflection coefficient A at point O as shown in Fig.1. Coefficient A is determined from the reflection and specular scattering coefficients and divergence factor. Polarization enters the model via the reflection coefficient. Standard formulas [29] relate the flat–earth quantities to the spherical–earth quantities.

The geometry for the radar model is illustrated in Fig.2. We consider four separate propagation paths for each element in the array: direct and reflected signals going from the transmitter to the target and direct and reflected signals returning from the target to the receiving array. We use small angle approximations [30] to derive the signal received at the k$^{\text{th}}$ element of the array:

$$v_k = Q_2 \, exp(-j2\xi R) \, exp\{-j\xi(z_k^2 + h_k^2)/2R\} \, exp\{-j\xi(z_e^2 + h_e^2)/2R\} \times [exp(j\xi h_k z_k/R) + A_2 \, exp(-j\xi h_k z_k/R)][exp(j\xi h_e z_e/R) + A_1 \, exp(-j\xi h_e z_e/R)] \tag{2.2}$$

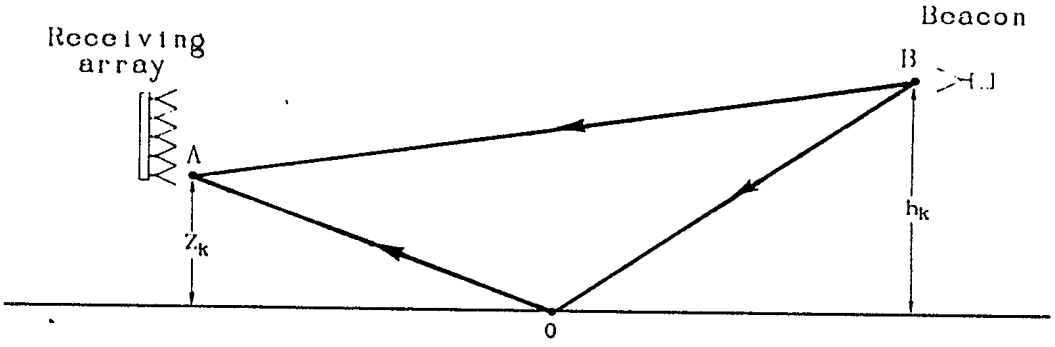

Figure 1: Geometry for the beacon model

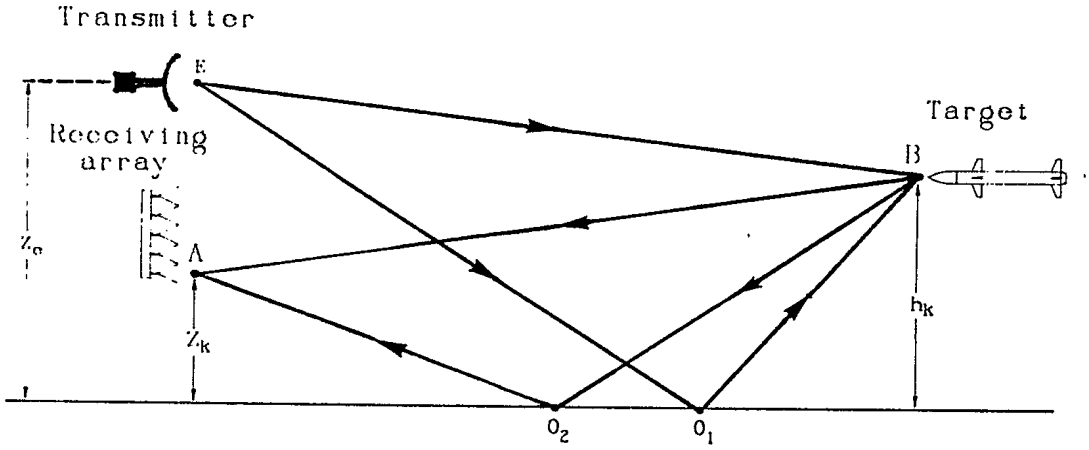

Figure 2: Geometry for the radar model

where z_e and h_e are the transmitter and target heights with respect to the tangent plane at the reflection point O_1 for the transmitted signal; Q_2 is an unknown complex amplitude due to target characteristics; z_k and h_k are the height of the k^{th} antenna element and that of the target measured with respect to the tangent plane at the reflection point, O_2, for the signal returning from the target; and A_1, A_2 are the complex multipath reflection coefficients at point O_1 and O_2 respectively. All the quantities are corrected for the earth curvature and these corrections are different for each antenna element height. Therefore, we represent the target height by h_k.

To simplify the notation let:

$$v_k = b\, f_k(h) \tag{2.3}$$

where $$b = Q_1\, exp(-j\xi R) \qquad \text{(beacon model)} \tag{2.3a}$$

or $$b = Q_2\, exp(-j2\xi R)\, exp\{-j\xi(z_e^2 + h_e^2)/2R\} \times [exp(j\xi h_e z_e/R) + A_1\, exp(-j\xi h_e z_e/R)] \qquad \text{(radar model)} \tag{2.3b}$$

and $$f_k(h) = exp\{-j\xi(z_k^2 + h_k^2)/2R\}\, [exp(j\xi h_k z_k/R) + A_2\, exp(-j\xi h_k z_k/R)]$$ (same for both beacon and radar model) (2.3c)

Assume that the observation vector or snapshot $\mathbf{s}$ coming from the output of an array having K sensors is given by

$$\mathbf{s} = b\, \mathbf{f}(h) + \boldsymbol{\eta} \tag{2.4}$$

with $(\mathbf{s}, \mathbf{f}, \boldsymbol{\eta}) \in \mathbb{C}^{K*1}$, $b \in \mathbb{C}^{1*1}$ and where b can be deterministic (non–fluctuating case) or random (fluctuating case) and the noise vector $\boldsymbol{\eta}$ is assumed to be stationary, additive, spatially white and independent of the target signals.

3 The RML technique

The ML estimate of an unknown parameter vector $\boldsymbol{\theta}$ is that value of $\boldsymbol{\theta}$ which maximizes the conditional density $p(\boldsymbol{s}|\,\boldsymbol{\theta})$ of the observations, or likelihood function. The RML technique uses ML estimation with a model that accounts for the physics of specular

multipath. Depending on the degree of coherence between snapshots, different estimators are derived. We consider three cases:

1) N coherent snapshots;
2) M non–coherent snapshots;
3) M non–coherent trains of N_m coherent snapshots.

3.1 N coherent snapshots:

We achieve signal coherence by using a coherent radar of good quality in order to describe the relative phase shift between the signal component of the snapshots in terms of the doppler shift caused by target motion between signal snapshots. Pulse–Doppler radars may use pulse repetition frequencies as high as 25 kHz in some instances although frequencies of 10 kHz or less are more usual. The degree of signal coherence in these radars is necessarily high to achieve strong clutter rejection. We reject clutter by using Doppler filtering. The target speed is obtained by identifying the particular Doppler filter output which gives rise to a detection.

The observation model is given by

$$\mathbf{s}_n = b_n \mathbf{f}_n(h) + \eta_n \tag{3.1}$$

where

$\mathbf{s}_n$: represents the n^{th} snapshot;
$b_n = b \exp(j\varphi_n)$ with φ_n the known Doppler phase shift (determined by Doppler filtering).

The ML estimate of $\boldsymbol{\theta}$ is that value of $\boldsymbol{\theta}$ which maximizes the conditional joint density (i.e. likelihood function) or a monotonic function of it (i.e. log–likelihood). The conditional joint density is given by

$$p(\mathbf{s}_1,\mathbf{s}_2,\ldots,\mathbf{s}_N \mid \boldsymbol{\theta}) = \prod_{n=1}^{N} C \exp\{-(\mathbf{s}_n - b_n \mathbf{f}_n)^H (\mathbf{s}_n - b_n \mathbf{f}_n)\}/\sigma_n^2 \tag{3.2}$$

where C does not depend upon parameter vector $\boldsymbol{\theta}$ and N is the total number of snapshots.

The log–likelihood function for this case, after dropping the constants independent of $\boldsymbol{\theta}$, is

$$L(\boldsymbol{\theta}) = -\sum_{n=1}^{N} \|\mathbf{s}_n - b_n\, \mathbf{f}_n(h)\|^2/\sigma_n^2 \tag{3.3}$$

with $\boldsymbol{\theta} = [h,\ b]$.

We may assume that the model $\mathbf{f}_n(h)$ and the noise power do not change appreciably over a period of several milliseconds so that $\mathbf{f}_n(h)$ can be replaced by $\mathbf{f}(h)$ and σ_n^2 by σ^2. The log–likelihood function becomes

$$L(\boldsymbol{\theta}) = -\sum_{n=1}^{N} \|\mathbf{v}_n - b\, \mathbf{f}(h)\|^2/\sigma^2 \tag{3.4}$$

with

$$\mathbf{v}_n = \mathbf{s}_n\, exp(-j\varphi_n) \tag{3.4a}$$

Here, we have replaced b_n by $b\ exp(j\varphi_n)$.

Now let

$$\mathbf{s}_S = \sum_{n=1}^{N} \mathbf{v}_n \tag{3.5}$$

where $\mathbf{s}_S$ is the coherent integration of the signal component in the N snapshots $\mathbf{s}_n$.

Vector $\mathbf{s}_S$ can always be formed if we know φ_n. It is the a priori knowledge of the φ_n which defines the snapshots as coherent. The equation (3.4) can now be written as

$$L(\boldsymbol{\theta}) = -\frac{1}{\sigma^2}\left[\sum_{n=1}^{N}\|\mathbf{v}_n\|^2 - b\, \mathbf{s}_S^H\mathbf{f} - b^*\, \mathbf{f}^H\mathbf{s}_S + N\, \|b\|^2\, \|\mathbf{f}\|^2\right] \tag{3.6}$$

A necessary condition for $L(\boldsymbol{\theta})$ to be maximized is obtained by setting the partial derivative of (3.6) with respect to b [31] to zero. This condition yields an estimate of b as

$$\hat{b} = \frac{(\mathbf{f}^H \mathbf{s}_s)}{N\|\mathbf{f}\|^2} \tag{3.7}$$

Substituting (3.7) in (3.6), we obtain the ML estimator of the height of a low–altitude target as the value of h that maximizes the following function:

$$C^c(h) = \frac{\|\mathbf{s}_s^H \mathbf{f}(h)\|^2}{N(\sum_{n=1}^{N} \|\mathbf{s}_n\|^2)\|\mathbf{f}(h)\|^2} \tag{3.8}$$

where the superscript ^{c} means coherent.

We determine the ML estimate of h by adjusting h in $C^c(h)$ until we find the largest peak. The summation of the squared magnitudes of the $\mathbf{s}_n$ snapshots in the denominator of $C^c(h)$ is simply a scaling factor which can be replaced by $\|\mathbf{s}_s\|^2/N$. In this case, the estimator has exactly the same form as obtained for a single snapshot except that $\mathbf{s}$ is replaced by, $\mathbf{s}_s$, the coherent integration in (3.5). Using the Cauchy–Schwartz inequality, we show that

$$N \sum_{n=1}^{N} \|\mathbf{s}_n\|^2 = N \sum_{n=1}^{N} \|\mathbf{v}_n\|^2 \geq \|\sum_{n=1}^{N} \mathbf{v}_n\|^2 = \|\mathbf{s}_s\|^2 \tag{3.9}$$

and we always have ($0 \leq C^c(h) \leq 1$).

In Fig. 3 is an example of $C^c(h)$ obtained by simulation using the following parameters: a target range at 5 km, a target height of 40 m, a vertical array of 8 sensors having a 1 m aperture centered at a height of 9.5 m about water, a smooth sea, and a transmitted frequency of 10 GHz. We observe that $C^c(h)$ has multiple peaks and presents height ambiguities. This arises because the model is a mathematical description of the interference pattern resulting from the summation of a direct signal and a reflected or image signal. Since the separation of target and its image is many wavelengths, the two act as a two–element antenna array and the height ambiguities correspond to the grating lobes of this antenna. Since this interference pattern is being detected by an array and the period for the grating lobe repetition is slightly different for each element in the array, the true peak is in theory the largest but the neighbouring peaks are so close and the decay in amplitude so slow that the amplitude is not a reliable indicator when operating at a single frequency.

3.2 M non–coherent snapshots:

Non–coherence between data snapshots can have a variety of causes. One can deliberately create non–coherence by the use of frequency agility; an important benefit is the resolution of height ambiguities described in the previous section. Another cause of non–coherence is the large time separation between the sampling of groups of snapshots sometimes encountered with experimental systems. Still other causes are the lack of coherence between reference oscillators or the lack of knowledge of the target velocity.

We assume that the observation vectors are statistically independent from snapshot to snapshot. The noise levels may differ for each frequency as a result of the frequency dependence of the receiver noise figure. The observation model is given by

$$\mathbf{s}_m = b_m \mathbf{f}_m(h) + \boldsymbol{\eta}_m \tag{3.10}$$

The log–likelihood function for this case, after dropping the constants independent of $\boldsymbol{\theta}$, is

$$L(\boldsymbol{\theta}) = -\sum_{m=1}^{M} \|\mathbf{s}_m - b_m \mathbf{f}_m(h)\|^2/\sigma_m^2 \tag{3.11}$$

where $\boldsymbol{\theta} = [h, b_1, b_2, \ldots, b_M]$ and M is the number of snapshots taken at different frequencies.

A necessary condition for $L(\boldsymbol{\theta})$ to be maximized is satisfied by setting the partial derivative of (3.11) with respect to each b_m [31] to zero. This condition yields an estimate of b_m as

$$\hat{b}_m = \frac{(\mathbf{f}_m^H \mathbf{s}_m)}{\|\mathbf{f}_m\|^2} \qquad m=1,2,\ldots,M \tag{3.12}$$

Substituting (3.12) in (3.11), we obtain the ML estimator of the target height as the value of h that maximizes the following function:

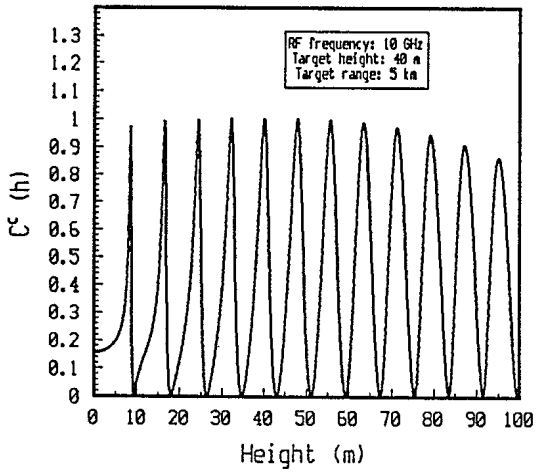

Figure 3 An example of $C^c(h)$

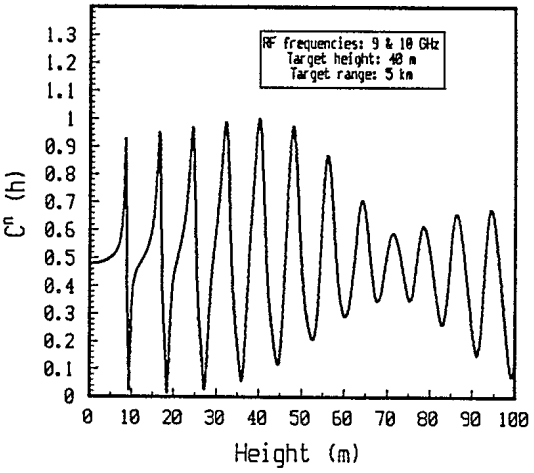

Figure 4: An example of $C^n(h)$

$$C^{n}(h) = \frac{1}{\sum_{m=1}^{M} \|s_m\|^2/\sigma_m^2} \sum_{m=1}^{M} \frac{\|s_m^H f_m(h)\|^2}{\sigma_m^2 \|f_m(h)\|^2} \tag{3.13}$$

where the superscript ^{n} means non coherent snapshots. By using the Cauchy–Schwartz inequality, we can show that $0 \leq C^{n}(h) \leq 1$.

In Fig. 4 is an example of $C^{n}(h)$ obtained by simulation using the same parameters as in Fig.3 but now with two transmitted radar frequencies of 9 and 10 GHz. Using more than two frequencies accentuates the value of the peak corresponding to the true target height relative to the ambiguous peaks [18]. The radar transmits a pulse at one frequency, changes frequency and transmits another pulse.

3.3 Mixed coherent and non–coherent snapshots:

The problem of mixed coherent and non–coherent snapshots occurs frequently in radar as a result of the use of burst–to–burst frequency agility. Here the radar transmits bursts of coherent pulses at one frequency, changes frequency and transmits another burst of pulses. Noise levels may differ on each pulse burst as a result of a frequency dependence of the receiver noise figure.

The observation model is given by

$$s_{nm} = b_{nm} f_{nm}(h) + \eta_{nm} \tag{3.14}$$

where m indicates the m^{th} frequency and n the n^{th} snapshot within a given coherent burst and $b_{nm} = b_m \, exp(j\varphi_{nm})$. Phase φ_{nm} represents the doppler shift as a result of target motion and is assumed known to within a constant α_m. Note that the unknown α_m is lumped into the complex constant b_m. Therefore, there is coherence within a burst. The α_m are unknown however, so that there is no coherence between bursts at different frequencies (different values of m). Because we assume coherence within the m^{th} burst, we can write $f_{nm}(h) = f_m(h)$ and consider a variable level of receiver noise represented by σ_m^2 for each burst. If φ_{nm} is not known, the model reduces to the completely non–coherent case of the previous section.

The conditional joint density to be maximized is $p(\mathbf{s}_{nm}|\,\boldsymbol{\theta})$ with n=1,2,...,N_m and m=1,2,...,M where N_m indicates the number of snapshots in the m^{th} burst and M is the number of different frequencies. The log–likelihood function is then

$$L(\boldsymbol{\theta}) = -\sum_{m=1}^{M} \frac{1}{\sigma_m^2}\left[\sum_{n=1}^{N_m} \|\mathbf{s}_{nm}\|^2 - b_m \mathbf{s}_{sm}^H \mathbf{f}_m - b_m^* \mathbf{f}_m^H \mathbf{s}_{sm} + N\,\|b_m\|^2\,\|\mathbf{f}_m\|^2\right] \tag{3.15}$$

$\boldsymbol{\theta}$ is defined as in the previous section.

σ_m^2 = noise power for the m^{th} frequency.

$\mathbf{s}_{sm} = \sum_{n=1}^{N_m} \mathbf{v}_{nm}$ = coherent integration of the N_m snapshots at the m^{th} frequency.

Following the same procedures as in the previous section to eliminate b_m of (3.15), we obtain the ML estimate of the height as the value of h that maximizes the following function:

$$C^{mx}(h) = \frac{1}{\sum_{m=1}^{M}\sum_{n=1}^{N_m} \|\mathbf{s}_{nm}\|^2/\sigma_m^2} \sum_{m=1}^{M} \left(\frac{\|\ \mathbf{s}_{sm}^H \mathbf{f}_m\|^2}{N_m \sigma_m^2 \|\mathbf{f}_m\|^2}\right) \tag{3.16}$$

The superscript ^{mx} means mixed case of coherent and non–coherent snapshots.

4 Formulation of the Cramer–Rao bound

The Cramer–Rao bound is a lower bound to the variance of an unbiased estimate. Most estimators have biases if the number of samples is small and/or the signal–to–noise ratio small. The Cramer–Rao bound is nevertheless considered an important indicator of performance of ML estimators because (i) ML estimators are asymptotically unbiased as the number of samples increases and (ii) the variance of ML estimators approaches the CR bound asymptotically as the number of samples increases [32].

The Cramer–Rao bound is formulated in terms of the Fisher information matrix **J** [32], the dimension of which depends on the number of unknown parameters in the likelihood function. For example, when the data vectors are coherently integrated into a

single data vector, there are three unknown target parameters, height h, signal amplitude r, and signal phase ψ. **J** is then a 3×3 matrix. In comparison, the standard angle–of–arrival model has two unknown amplitudes, two unknown phases, and two unknown angles; **J** is then a 6×6 matrix. The $(i,j)^{th}$ element of **J** is given by

$$J_{ij} = -E\left\{\frac{\partial^2(log\ p(s|\theta))}{\partial\theta_i\ \partial\theta_j}\right\} \tag{4.1}$$

and if J^{ij} is the $(i,j)^{th}$ element of $\mathbf{J}^{-1}$ then the Cramer–Rao bound on the variance of the estimate of θ_i is:

$$\mathrm{Var}(\hat{\theta}_i - \theta_i) \geq J^{ii} \tag{4.2}$$

Consider the general observation model for the non–coherent snapshots (eq.3.10). The log–likelihood function is then

$$L(\theta) = -\sum_{m=1}^{M} \frac{1}{\sigma_m^2} (\mathbf{s}_m - \mathbf{g}_m(\theta))^H (\mathbf{s}_m - \mathbf{g}_m(\theta)) \tag{4.3}$$

with $\mathbf{g}_m(\theta) = b_m \mathbf{f}_m(h)$, $b_m = r_m\ exp(j\psi_m)$ and where $\theta = [h, r_1, \psi_1, r_2, \psi_2, \ldots, r_M, \psi_M]$

Taking partial derivatives and the expectation as indicated in (4.1) leads to the following formula [33] for the Fisher information matrix:

$$\mathbf{J} = 2 \sum_{m=1}^{M} \frac{1}{\sigma_m^2} \mathrm{Re}(\mathbf{H}_m^H \mathbf{H}_m) \qquad \in \mathbb{R}^{L*L} \tag{4.4a}$$

with

$$\mathbf{H}_m = \left[\frac{\partial \mathbf{g}_m(\theta)}{\partial\theta_1} \quad \frac{\partial \mathbf{g}_m(\theta)}{\partial\theta_2} \quad \ldots \quad \frac{\partial \mathbf{g}_m(\theta)}{\partial\theta_L} \right] \qquad \in \mathbb{C}^{K*L} \tag{4.4b}$$

and where L is the number of real unknown parameters (2M+1) and K indicates the number of sensors.

There is a total of $L = (2M+1)$ unknowns: h, $\{r_1, r_2, \ldots, r_M\}$, $\{\psi_1, \psi_2, \ldots, \psi_M\}$. The matrix $\mathbf{H}_m$ has dimension $K \times (2M+1)$ and there are only three columns with non–zero values because

$$\frac{\partial f_{kn} b_n}{\partial \psi_m} = \frac{\partial f_{kn} b_n}{\partial r_m} = 0 \qquad \text{if } m \neq n \tag{4.4c}$$

Now, partition $\mathbf{J}$ as

$$\mathbf{J} = 2 \left[\begin{array}{c|ccccc} \sum_{m=1}^{M} g_{1m} & \mathbf{g}_{21}^T & \mathbf{g}_{22}^T & \cdots & & \mathbf{g}_{2M}^T \\ \hline \mathbf{g}_{21} & \mathbf{G}_{31} & & & & \\ \mathbf{g}_{22} & & \mathbf{G}_{32} & & & \\ \vdots & & & \ddots & & \\ \mathbf{g}_{2M} & & & & & \mathbf{G}_{3M} \end{array}\right] \tag{4.5}$$

where $g_{1m} \in \mathbb{R}^{1*1}$, $\mathbf{g}_{2m} \in \mathbb{R}^{1*2}$, $\mathbf{G}_{3m} \in \mathbb{R}^{2*2}$.

and with

$$g_{1m} = \frac{r_m^2}{\sigma_m^2} \left\| \frac{\partial \mathbf{f}_m}{\partial h} \right\|^2 \tag{4.5a}$$

$$\mathbf{g}_{2m} = \begin{bmatrix} -\dfrac{r_m^2}{\sigma_m^2} \mathrm{Im}\left[\dfrac{\partial \mathbf{f}_m^H}{\partial h} \mathbf{f}_m \right] \\ \dfrac{r_m^2}{\sigma_m^2} \mathrm{Re}\left[\dfrac{\partial \mathbf{f}_m^H}{\partial h} \mathbf{f}_m \right] \end{bmatrix} \tag{4.5b}$$

$$G_{3m} = \begin{bmatrix} \frac{r_m^2}{\sigma_m^2} & 0 \\ 0 & \frac{\|f_m\|^2}{\sigma_m^2} \end{bmatrix} \tag{4.5c}$$

Using the matrix inversion lemma [34, p.41], the Cramer–Rao bound on the variance of the target height estimate is

$$\mathrm{CRB}(\hat{h}) \geq \frac{1}{2\sum_{m=1}^{M} \mathrm{SNR}_m \left[\left\| \frac{\partial f_m}{\partial h} \right\|^2 - \frac{1}{\|f_m\|^2} \left\| \frac{\partial f_m^H}{\partial h} f_m \right\|^2 \right]} \tag{4.6a}$$

with

$$\mathrm{SNR}_m = \frac{r_m^2}{\sigma_m^2} \tag{4.6b}$$

We illustrate the Cramer–Rao bound for data vectors that are coherently integrated into a single data vector by setting M = 1 in (4.6a). Fig. 5 shows the Cramer–Rao bound multiplied by SNR and plotted versus target height for a target at 5 km, a radar wavelength of 3 cm and for various values of the amplitude of the reflection coefficient, a, and assuming horizontal polarization. The horizontal line represents the case where a = *0*. This case corresponds to the best that can be done with a model using a single plane wave (monopulse, Fourier beamforming). The limit obtained when a = *0*, can be shown to be equivalent to the Cramer–Rao limit of Rife and Boorstyn [35, eq.17] for the estimation of the frequency of a sinewave of unknown amplitude and phase, provided we interpret $\sin\theta$ as the spatial frequency and $2\pi d/\lambda$ as the interval between samples. The results of figure 5 indicate that, over a very wide range of target heights of interest, modelling the multipath by using two plane waves is a very significant aid in measuring target height if the appropriate models are used. Indeed, the curves for a=.5 and a=.9 cross the a=0 curve only at target heights of less than 5 m. At h=5 m, the angular separation between the image and the direct path signal is 1/25 of a beamwidth for an array 21 wavelengths in extent as used in the example of Fig.5 (8 elements with 3λ spacing).

Fig.5 shows the effect of sea state which is taken into account by reducing the reflection coefficient. The best performance, as indicated by the lowest Cramer–Rao bound, occurs for the lower sea states (smooth sea a=.9). The ratio of the CR bound for a=0 to that for a=.9 approaches 30 dB. We expect a similar ratio between the error variances for high SNR. As the smooth reflecting surface becomes rough, the strength of the specular multipath, a, decreases. We conjecture that for sufficiently rough seas, modelling the multipath may create more errors than using a model with only the direct signal. The effect of model errors is to produce a bias on the estimated target height.

5.0 Results of Monte–Carlo simulations

We have used the root–mean–square errors, RMSE, as the measure of performance. The results shown in Fig.6 use a linear array of K=8 equally spaced omnidirectional elements, with an antenna aperture of one–metre length. The height of the target was arbitrarily fixed at 10 metres and two X–band frequencies were used (9 and 10 GHz) operating over a smooth sea corresponding to Sea State 2 or lower. We carried out Monte–Carlo simulations to determine the threshold effects on height estimation. We have also plotted the Cramer–Rao bound. Our estimators lie very close to the Cramer–Rao limit for large SNR but large deviations occur as the SNR decreases below a threshold value.

The term SNR , is a per–element averaged quantity summed over the number of frequencies:

$$\mathrm{SNR}_{\mathrm{dB}} = 10 \log \left\{ \sum_{m=1}^{M} \frac{r_m^2 \, \| \mathbf{f}_m(h_t) \|^2}{2K \, \sigma_m^2} \right\} \tag{5.1}$$

where (M=2) is the number of frequencies, h_t=10 m is the target height and σ_m^2 is the noise power.

We have plotted on Fig.6, the Cramer–Rao bound and the estimator $C^n(h)$. Our estimator lies very close to the Cramer–Rao limit for large SNR but large deviations occur as the SNR decreases below a threshold value. To decrease this estimation threshold, we increase the number of frequencies and the frequency bandwidth.

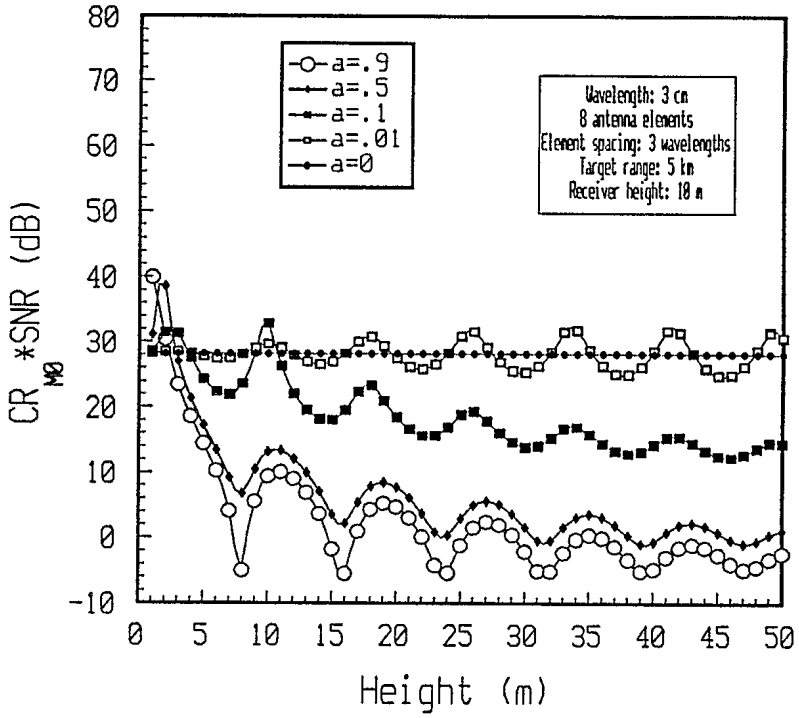

Figure 5: Comparison of CR bounds with various values of reflection coefficient

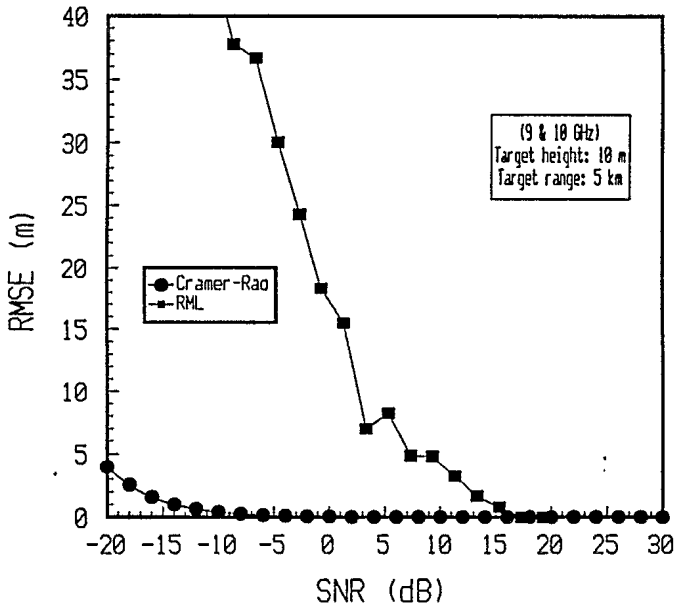

Figure 6: Threshold effects

6. EXPERIMENTAL RESULTS.

The performance of the RML technique has been evaluated with two experimental systems: the ELAT and the MARS systems. The ELAT results are presented in Figs. 7 to 11. Each figure has three parts: 1) estimated SNR, 2) FFT beamforming results, 3) the RML results.

We estimate the noise power by using a projection technique to remove the specular component as

$$\hat{\mathbf{n}}_m = \mathbf{s}_m - \frac{(\mathbf{f}_m^H(\hat{h}_t)\mathbf{s}_m)}{\|\mathbf{f}_m(\hat{h}_t)\|^2}\mathbf{f}_m(\hat{h}_t) \tag{6.1}$$

where $\hat{h}_t$ is the ML estimate of the target height obtained from our analysis of $C^n(h)$. The quantity $\|\hat{\mathbf{n}}_m\|^2$ is an estimate of the combined power of the receiver noise and the diffuse multipath for the m^{th} frequency.

The estimated SNR is then given by the following equation:

$$\hat{\text{SNR}}(\text{dB}) = 10\,log\left\{\sum_{m=1}^{M}\frac{\|\mathbf{s}_m\|^2 - \|\hat{\mathbf{n}}_m\|^2}{\|\hat{\mathbf{n}}_m\|^2}\right\} \tag{6.2}$$

The estimate given by (6.2) is in reality the ML estimation of SNR. By the invariance property of ML estimators [36, p.92], we have that $\mathbf{g}(\hat{\theta}_{ML})$ is the ML estimate of $\mathbf{g}(\theta)$. If we apply this property to our case the ML estimate of the mean $b_m\mathbf{f}_m(h_t)$ is given by

$$\hat{\mu}_m = \mathbf{g}(\hat{\theta}_{ML}) = \hat{b}_m\mathbf{f}_m(\hat{h}_t) \tag{6.3}$$

with $\hat{b}_m$ given by the relation (3.12).

It is well known that the ML estimate of the mean of a Gaussian population is equal to the sample mean and the ML estimate of the variance of a Gaussian population is simply equal to the sample variance [36, p.91]. The noise variance is then given by

$$\hat{\sigma}_m^2 = \|s_m - \hat{\mu}_m\|^2 \tag{6.4}$$

When we compare (6.4) with the amplitude squared of (6.1), we conclude that the projection method yields the ML estimate of the noise power σ_m^2.

The middle part on each figure presents results obtained with the classical Fourier beamforming. We choose to compare our results with those of Fourier beamforming because Fourier beamforming produces angular tracking errors comparable to monopulse, the most widely used tracking radar. It is anticipated that superresolution algorithms [6–7], when applicable to low–angle tracking, produces angular tracking errors between those obtained with Fourier beamforming and the RML technique. This topic will be covered in a subsequent paper.

The results for conventional beamforming are obtained by forming beams directly to obtain an estimate of the target height. The set of the eight sensor outputs collected at a particular instant of time are augmented with zeros to form a complex vector of 1024 points. We use the Fast Fourier Transform (FFT) in the angular domain to obtain an estimate of the elevation angle, which is converted to a height estimate. This is repeated for the second operating frequency and the final estimate is an average of the two estimates. This feature significantly improves the estimation performance compared with single–frequency conventional beamforming; the results of which are not shown here.

The bottom part of each figure presents results obtained using the RML technique with the estimator $C^n(h)$.

6.1 Experimental results using the ELAT system:

This section presents examples of experimental target tracking using the ELAT radar. ELAT is being developed at DREO as part of a research program into high angular resolution techniques for radar. The ELAT radar is designed with a sampled aperture antenna composed of 8 receiving elements spaced at a distance of 14 cm. Each element is connected to an individual receiver for conversion of 8.65 or 9.6 GHz microwave frequency information to the video frequency band. Each receiver includes quadrature (Q) and in–phase (I) detectors which are followed by analog–to–digital conversion in each channel. Using this receiving arrangement, discrete samples of the electromagnetic field across the

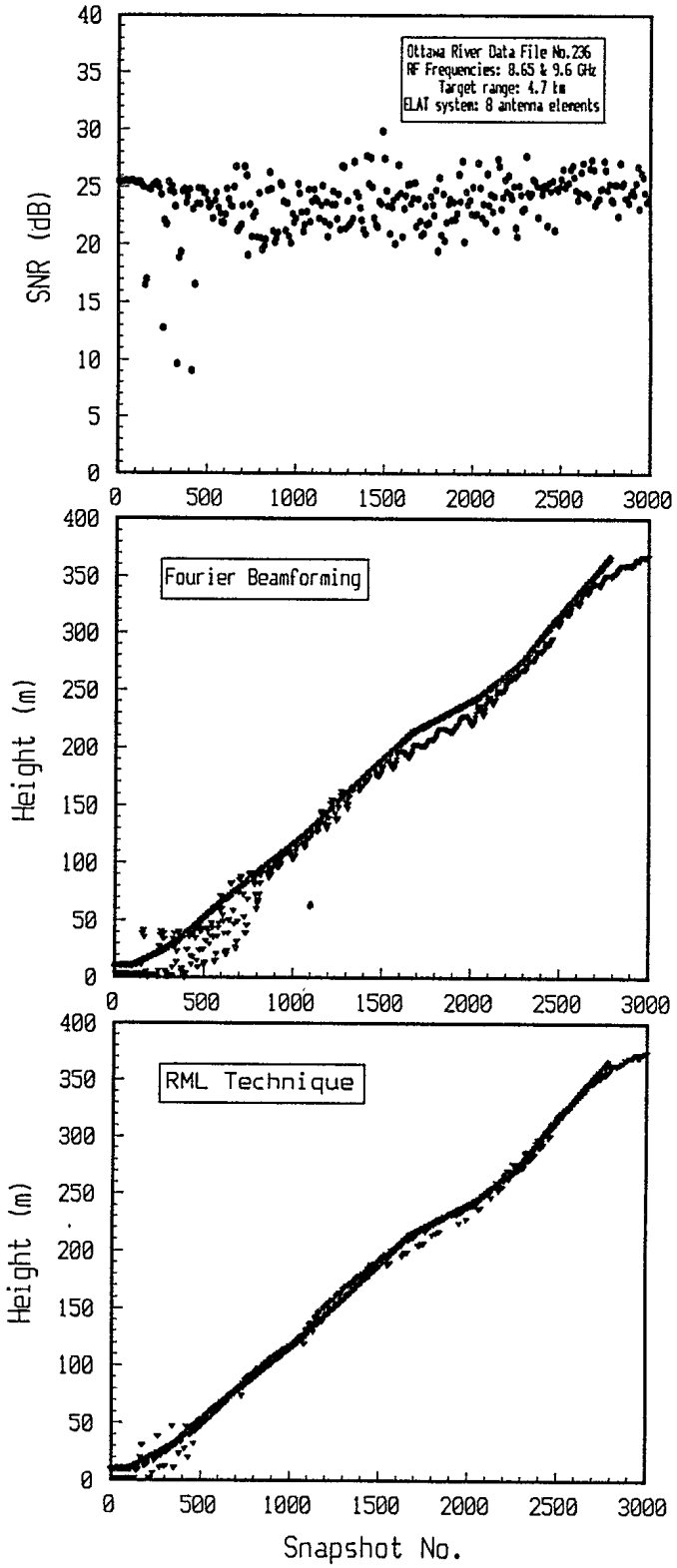

Figure 7: Tracking an ascending target over smooth sea (SS1)

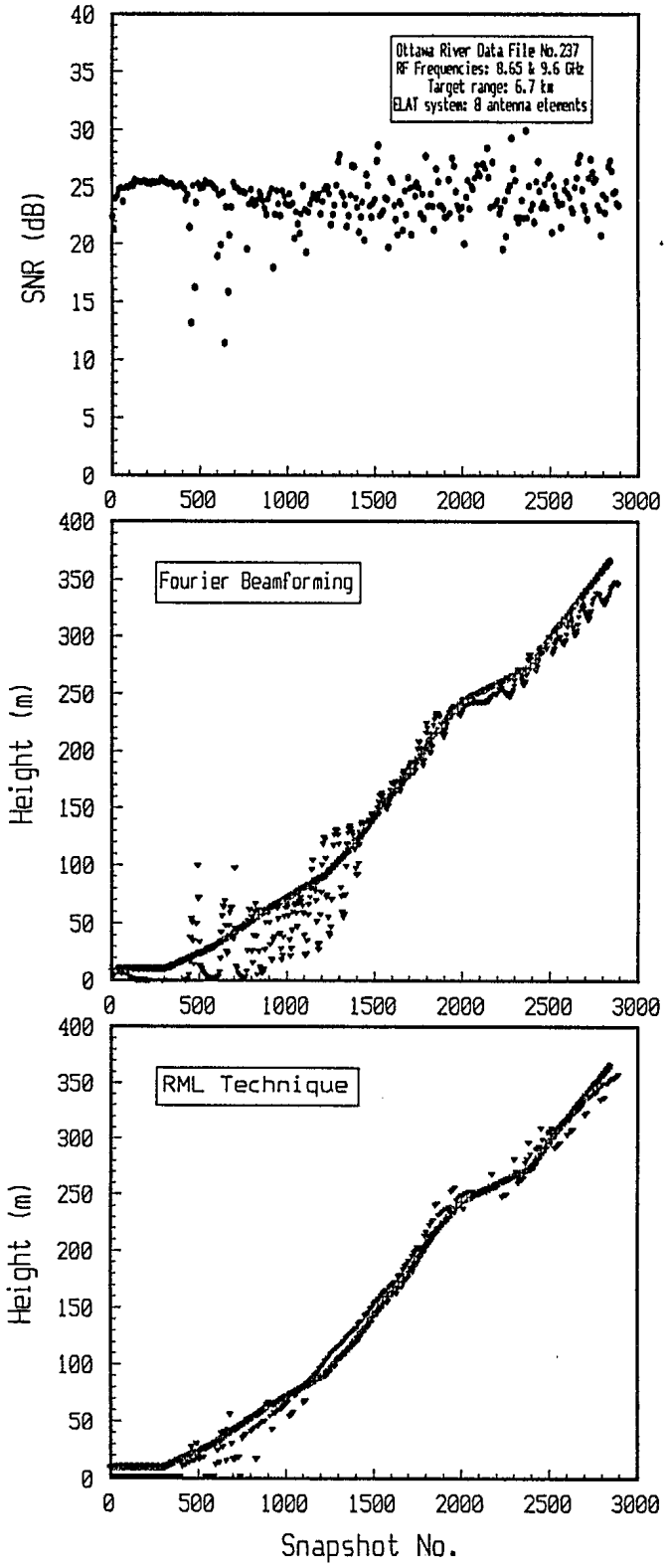

Figure 8: Tracking an ascending target over smooth sea (SS1)

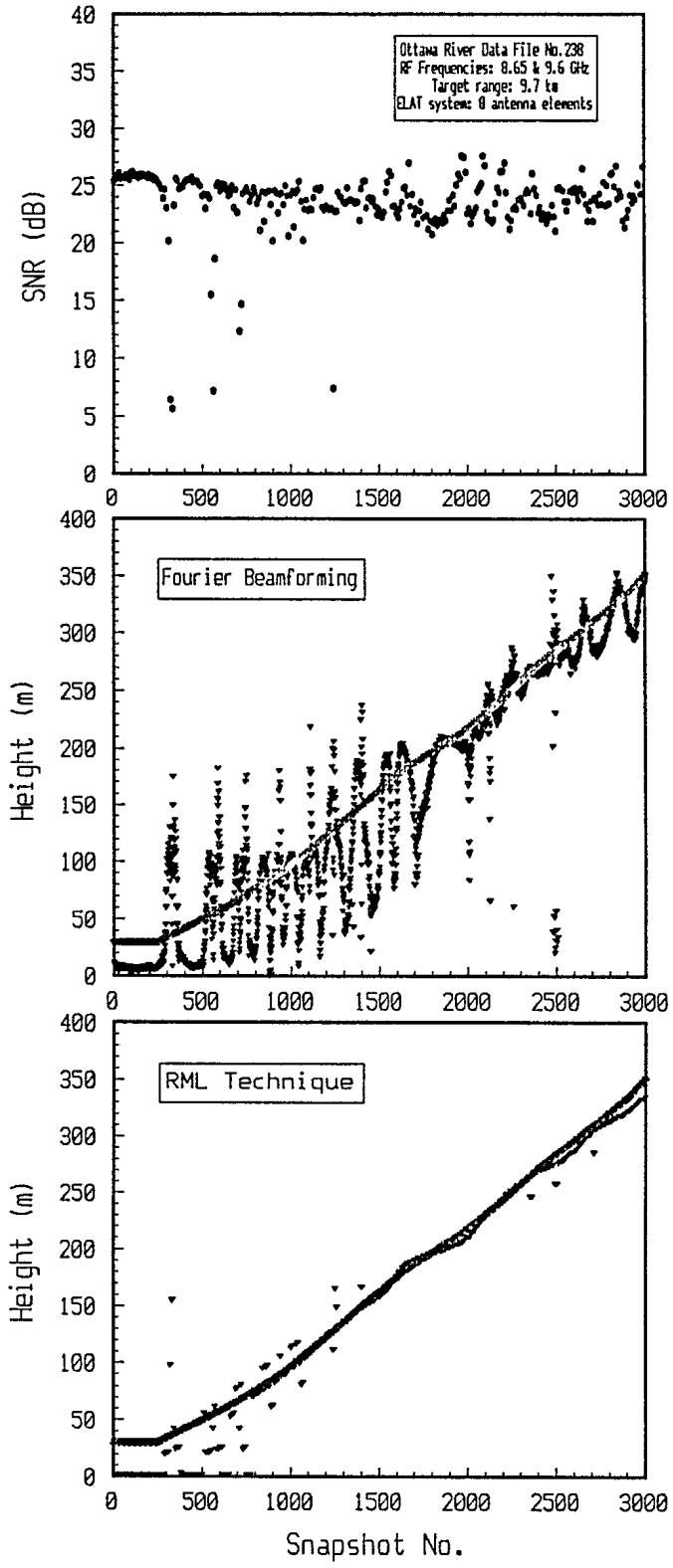

Figure 9: Tracking an ascending target over smooth sea (SS1)

vertical antenna aperture can be converted to the video band to form the observation vector or snapshot s, used in the previous sections.

To test $C^n(h)$ we use five files collected on the Ottawa River. We have installed a beacon in a low–flying helicopter. The two frequencies used are 8.65 and 9.6 GHz. For the first three examples the helicopter moves vertically from approximately 10 m to 350 m. This profile is repeated for three different ranges (4.7 km, 6.7 km, 9.7 km). The other two files represent a target manoeuvring in height over a 15 km path with the helicopter flying toward the vertical array. The solid line on each figure represents the theoretical pattern that the pilot tried to follow.

From Figs.7–9, we can make the following observations:

1. The variance on the height estimation increases with range (Fig.9 compared to Fig.7);

2. The RML method using $C^n(h)$ gives superior results when compared to Fourier beamforming specially at low altitude, and

3. Fourier beamforming gives useful estimates only when the angular separation between the target and its image is one beamwidth or larger. In this example, one beamwidth is approximately equal to 0.034 ($=\lambda/D$, where D is the array aperture) radians, corresponding to a target height of 80 m at 4.7 km or 160 m at 9.7 km.

The next two figures, Figs.10–11, present the tracking over a 15 km path. The results indicate that our technique gives an useful estimate of the target height while the classical Fourier beamforming produced poor target height estimates. The results obtained with the RML technique are relatively good considering that the data have been collected on the Ottawa River over a propagation path that was probably non–homogeneous due to the proximity of land.

6.2 Experimental results using the MARS system

The performance of the RML algorithm increases when using a larger bandwidth and multiple frequencies. This is in agreement with the experiment results derived from data collected by McMaster University at a site on Lake Huron using an array system

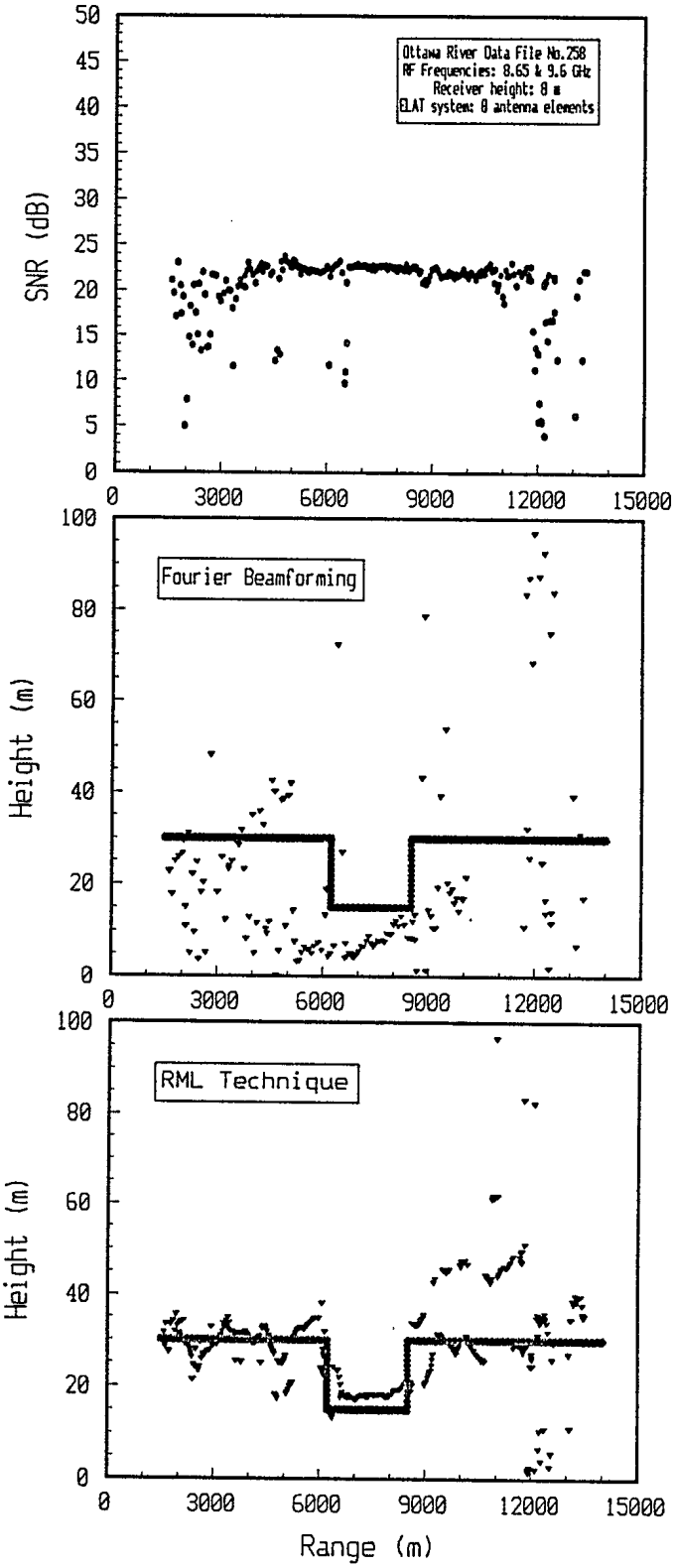

Figure 10: Tracking a target maneuvering over smooth sea (SS1)

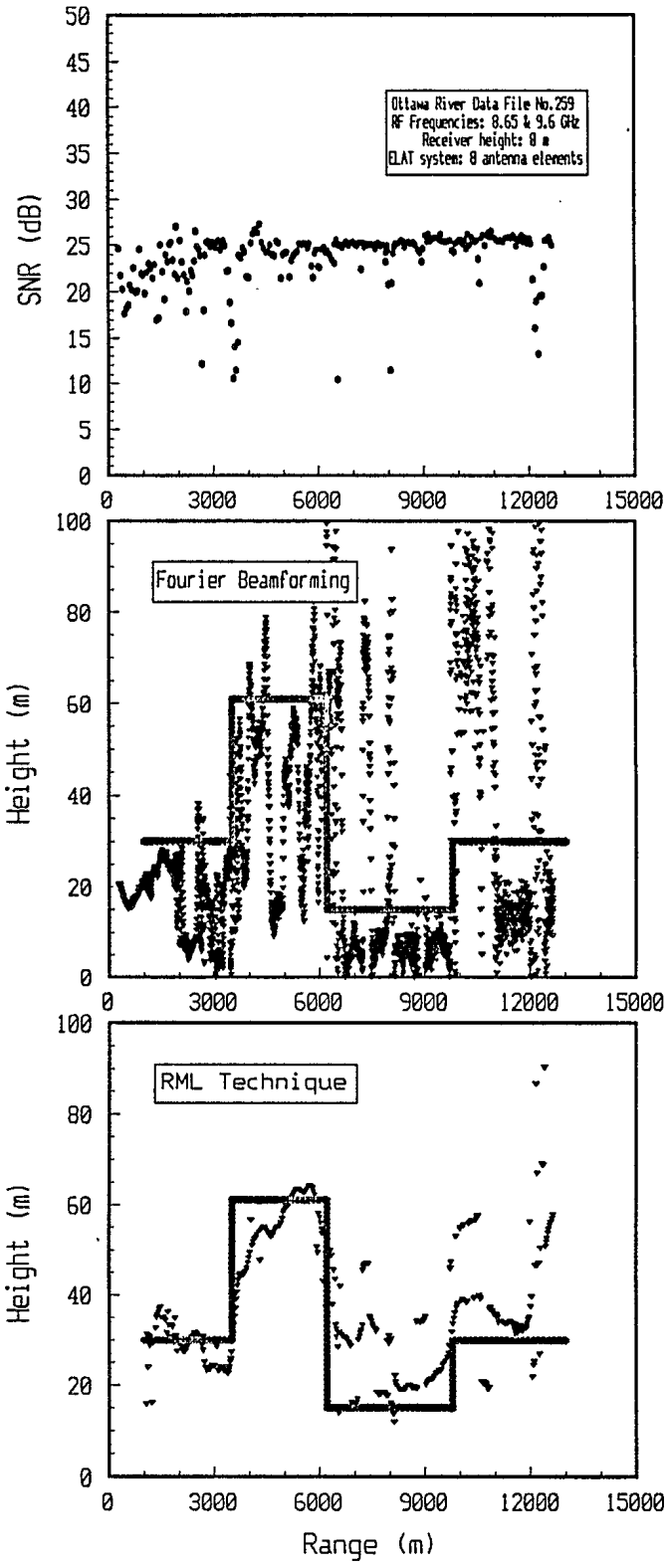

Figure 11: Tracking a target maneuvering over smooth sea (SS1)

called MARS. The MARS system comprises a multiple frequency beacon system, a sampled–aperture antenna and a data acquisition system. Two frequencies are simultaneously used for transmission: a fixed frequency of 10.2 GHz and an agile frequency ranging from 8.02 to 12.4 GHz in 30–MHz steps. In the experiments, only 18 frequencies were actually used. The sampled aperture contains a linear array of 32 elements uniformly spaced over a 1.82 m aperture. Each antenna element has its own receiver and the data are digitized with 12–bit precision.

For the Lake Huron experiments [12–13], the transmitter was sited at a distance of 4610 m from the receiving antenna. Fig.12 is a picture of the measurement setup. The height of the transmitter can vary from 2.7 m to 18.6 m above the water level. The height of the waves was visually observed to be about 1.5 m to 2 m (valley to peak) corresponding to a sea state of 3.

In Fig.13 we present the results obtained with a target varying its height from 3.5 m (.1 beamwidth) to 15.5 m (.4 beamwidth). The target range is 4610.4 m. The theoretical values are indicated by the solid line in the figure while the estimated target heights are indicated by a small triangle. We observe that the variance increases when the angular separation between the target and its image decreases. Biases are observed in all results. The results are obtained over a moderately rough sea surface (SS3) characterized by visual information and bias is created if the sea state is over or under estimated. Finally tilt and vibrations caused by strong wind (18 km/hr) contribute to both bias and the variance on the estimation. In Fig.14, both the variance and the bias decrease when we increase the bandwidth and the number of frequencies. The SNR estimated for the examples presented in Figs.13–14 is approximately 30 dB.

7. CONCLUSION

We have presented the theory for a new form of maximum likelihood estimation for low–angle tracking. This method is based on a "refined" propagation model employing a priori information; we have, therefore, coined the name Refined Maximum Likelihood (RML). The results of simulations and experiments with beacon signals indicate substantial improvements compared with previous techniques. However, the RML model is imperfect; it does not include diffuse multipath, sea swell or ducting. The results of limited experiments with beacons systems in estimated sea state 3 conditions are encouraging and

indicate some robustness in the presence of diffuse multipath. More extensive experimentation with radar signals is required to corroborate these results and to determine the applicability of the RML and the limitations of this applicability in realistic environments. Finally we want to emphasize the benefits of wide band frequency agility for effective resolution of ambiguities.

8. ACKNOWLEDGMENTS

The authors acknowledge assistance provided by Mr. Ed Riseborough in processing the experimental data. We also thank Dr. Eric Hung who reviewed this report.

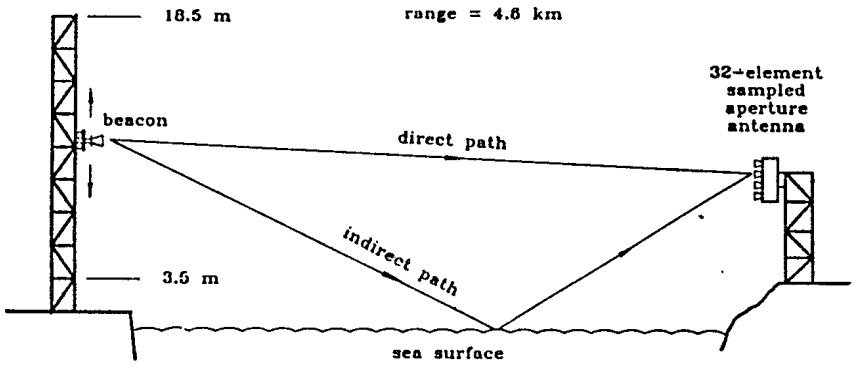

Figure 12: Geometry of the Lake Huron experimental setup

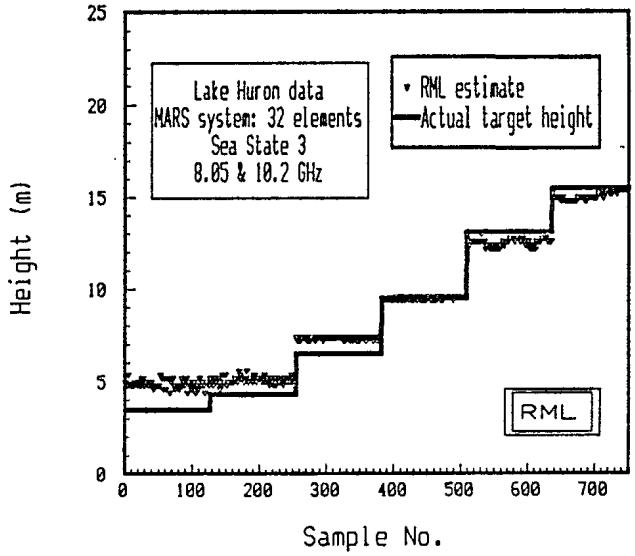

Figure 13: Example of tracking over relatively rough sea (SS3)

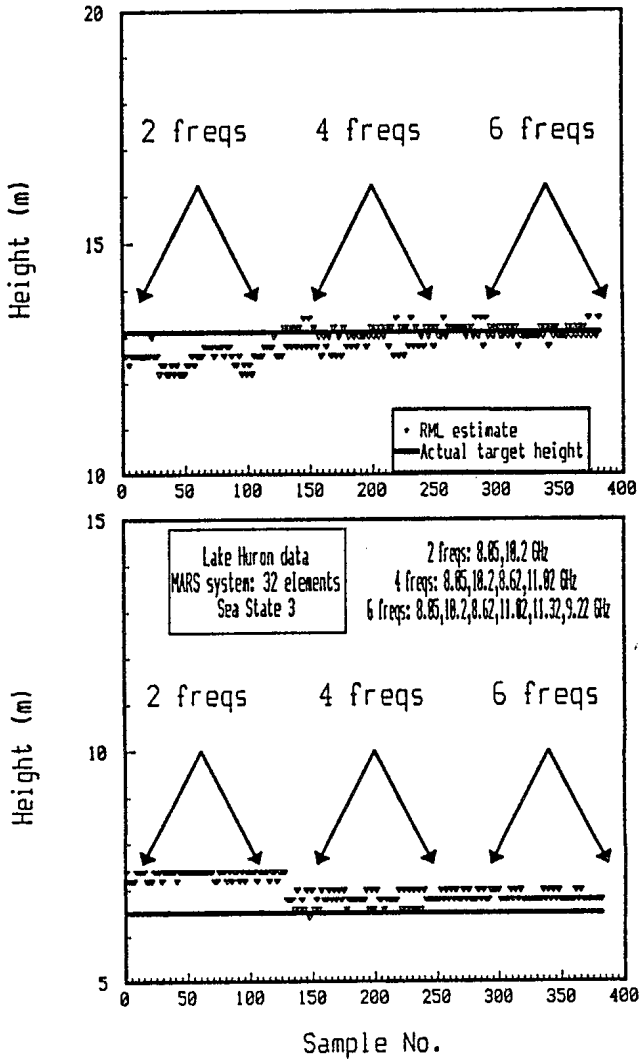

Figure 14: Effects of frequency agility on tracking (SS3)

9. REFERENCES:

[1] Barton, D. K., " Low–Angle Radar Tracking ", Proceedings IEEE, vol.62, no. 6 pp. 687–704, June 1974.

[2] Kesler, J., Haykin, S., " A New Adaptive Antenna for Elevation Angle Estimation in the Presence of Multipath ", Proc. IEEE AP–S Int. Symp., Québec, pp. 130–133 June 1980.

[3] Haykin, S., Kesler, J., " Adaptive Canceller for Elevation Angle Estimation in the Presence of Multipath ", IEE Proc. F, Commun., Radar and Signal Processing, vol.130, pp.303–308, June 1983.

[4] Haykin, S., " Array Signal Processing ", S.Haykin ed., Prentice Hall, Englewood Cliffs, NJ, 1985.

[5] Billam, McWhirter, Breems, Shore, Turner, Gröger, Nickel, Wirth, " Antenna Array Signal Processing in Phased Array Radar ", NATO Report, AC/243 (Panel 3 /RSG.15) D/8, p.105, May 1988.

[6] Nickel, U. " Angular Superresolution with Phased Array Radar: a Review of Algorithms and Operational Constraints ", IEE Proc., vol.134, Pt. F, no.1, pp.53–59, Feb. 1982.

[7] Johnson, R.L., Miner, G.E., " Comparison of Superresolution Algorithms for Radio Direction Finding ", IEEE Trans. on Aerospace and Electronic Systems, vol. AES–22, no.4, pp.432–441, July 1986.

[8] Pillai, S.U, Kwon, B.H., " Performance Analysis of MUSIC–Type High Resolution Estimators for Direction Finding in Correlated and Coherent Scenes ", IEEE Trans. on ASSP, vol. 37, no.8, pp.1176–1189, Aug. 1989.

[9] Zoltowski, M., Haber, F., " A Vector Space Approach to Direction Finding in a Coherent Multipath Environment ", IEEE Trans. AP, vol. 34, pp.1069–1079, Sept.1986.

[10] Grenier, D., " Application du Traitement du Signal à l'analyse Spatiale de Sources Corrélées à Bande Étroite ", Ph.D Thesis, Université Laval, Qué., Feb. 1989.

[11] Litva, J., " Early results: Very Low–Level Propagation Measurements on the Ottawa River ", IEEE Trans. on Antennas and Propagation, Vol. AP–35, No.4, Apr.1987.

[12] Lo, T., Lai, L., Litva, J., " Validation of a Sea Swell Model, Analysis of Real Multipath Data and Testing of the CHA Technique with Real and Simulated Data ", CRL Report, (under review), McMaster University, Hamilton, March 1990.

[13] Bauman, P.,, Litva, J., Lai, L., Lo, T., " Sea–Swell Modeling, Collection and Analysis of Data ", CRL Report no.199, McMaster University, Hamilton, Ontario, March 1989.

[14] Litva, J., " A New Low–Angle Tracking Technique ", CRC Report No. 1335, Communications Research Centre, Ottawa, May 1980.

[15] Rook, B., Litva, J., " An Improved CHA Algorithm for Tracking Low Angle Targets ", CRC Report No. 1356, Communications Research Centre, Ottawa, May 1980.

[16] Litva, J., " Use of Highly Deterministic Model in Signal–Bearing Estimation ", Electronics Letters, vol.25, no.5, pp.346–348, March 1989.

[17] Turner, R.M, Bossé, E., " Maximum Likelihood Tracking Using a Highly Refined Multipath Model ", 21st Asilomar conference on Signals, Systems and Computers, Pacific Grove, CA, Nov.2–4, 1987.

[18] Bossé, E., Turner, R.M, " Height Ambiguities in Maximum Likelihood Estimation with a Multipath Propagation Model ", 22nd Asilomar Conference on Signals, Systems and Computers, Pacific Grove, CA, Oct. 31–Nov. 2, 1988.

[19] Turner, R.M., Bossé, E., " The Use of Highly Refined Propagation Models in Maximum Likelihood Estimation of Target Elevation for Radar Tracking of Low–Altitude Targets over the Sea ", EUSIPCO–88, Grenoble, Sept.5–8, 1988.

[20] Ballance, W., Jaffer, A.G., " Low–Angle Direction Finding Based on Maximum Likelihood: an Unification ", 21st Asilomar conference on Signals, Systems and Computers, Pacific Grove, CA, Nov.2–4, 1987.

[21] Ksienski, A.A, McGhee, " A Decision Theoretic Approach to the Angular Resolution and Parameter Estimation Problem for Multiple Targets ", IEEE Trans. on Aerosp. Electro. Syst. vol.AES–4, pp.443–455, May 1968.

[22] Pollon, G.E., Lank, G.W., " Angular Tracking of Two Closely Spaced Radar Targets ", IEEE Trans. on Aerosp. Electro. Syst. vol.AES–4, pp.541–550, July 1968.

[23] Howard, J.E, " A Low Angle Tracking System for Fire Control Radars ", IEEE Int.Radar Conf. Rec. Arlington, VA, PP.412–417, April 1975.

[24] Trunk, G.V, Cantrell, B.H., Gordon, W.B., " Probability Density of the Maximum Likelihood Elevation Estimate of Radar Targets ", IEEE Trans. on Aerosp. Electro. Syst. vol.AES–15, pp.288–290, March 1979.

[25] Cantrell, B.H., Gordon, W.B., Trunk, G.V, " Maximum Likelihood Elevation Angle Estimates of Radar Targets Using Subapertures ", IEEE Trans. on Aerosp. Electro. Syst. vol.AES–17, pp.213–221, March 1981.

[26] Reilly, J.P., " Nonlinear Array Processing Techniques with Applications to Correlated Multipath ", Ph.D Thesis, McMaster University, Hamilton, Ontario, March 1981.

[27] Haykin, S., Reilly, J.P., " Maximum Likelihood Receiver for Low–Angle Tracking Radar. Part 1: The Symmetric Case ", IEE Proc. F, Commun., Radar & Signal Process., vol.129, pp.261–272, Aug. 1982.

[28] Reilly, J.P., Haykin, S., " Maximum Likelihood Receiver for Low–Angle Tracking Radar. Part 2: The Nonsymmetric Case ", IEE Proc. F, Commun., Radar & Signal Process., vol.129, pp.331–340, Oct. 1982.

[29] Kerr, D.E, (Éditeur), " Propagation of Short Radio Waves ", Peter Peregrinus, London, U.K, 1987. (originally published by McGraw–Hill in 1951).

[30] Bossé, E., " Localisation radar de cibles rasantes utilisant le maximum de vraisemblance et la physique des phénomènes de propagation", Ph.D Thesis, Université Laval , Québec, 1990.

[31] Brandwood, D.H., " A Complex Gradient Operator and its Application in Adaptive Array Theory ", IEE Proc. F and H, Microwaves, Opt. Antennas, Vol. 130, pp.111–116, Feb. 1983.

[32] Kendall, M., Stuart, A., " The Advanced Theory of Statistics, vol.2, Inference and Relationship ", Oxford University Press, 4th ed, New–York, 1979.

[33] Ballance, W., Jaffer, A.G., " The Explicit Cramer–Rao Bound on Angle Estimation ", 22nd Asilomar Conference on Signals, Systems, and Computers, Pacific Grove, CA, Oct.31–Nov2, 1988.

[34] Noble, B., Daniel, J.," Applied Linear Algebra ", 3rd ed., Prentice–Hall, Englewood Cliffs, N.J., 1988.

[35] Rife, D.C, Boorstyn, R.R., " Multiple Tone Parameter Estimation from Discrete–Time Observations. ", Bell System Technical Journal, vol. 55, pp.1389–1410, Nov. 1976.

[36] Mendel, J.M., " Lessons in Digital Estimation Theory ", Prentice–Hall, Englewood Cliffs, New Jersey, 1987.

DOCUMENT CONTROL DATA

(Security classification of title, body of abstract and indexing annotation must be entered when the overall document is classified)

1. ORIGINATOR (the name and address of the organization preparing the document. Organizations for whom the document was prepared, e.g. Establishment sponsoring a contractor's report, or tasking agency, are entered in section 8.)

DEFENCE RESEARCH ESTABLISHMENT OTTAWA
3701 Carling Ave, Ottawa, K1A 0Z4

2. SECURITY CLASSIFICATION (overall security classification of the document. including special warning terms if applicable)

UNCLASSIFIED

3. TITLE (the complete document title as indicated on the title page. Its classification should be indicated by the appropriate abbreviation (S,C or U) in parentheses after the title.)

A Refined Maximum Likelihood Method for Tracking Low-Altitude Targets over the Sea: Results of Simulation and Experiments. (U)

4. AUTHORS (Last name, first name, middle initial)

Bosse, Eloi, Turner, Ross M., Brookes, Daniel E.

5. DATE OF PUBLICATION (month and year of publication of document)

December 1991

6a. NO. OF PAGES (total containing information. Include Annexes, Appendices, etc.)

40

6b. NO. OF REFS (total cited in document)

36

7. DESCRIPTIVE NOTES (the category of the document, e.g. technical report, technical note or memorandum. If appropriate, enter the type of report, e.g. interim, progress, summary, annual or final. Give the inclusive dates when a specific reporting period is covered.)

Technical Report

8. SPONSORING ACTIVITY (the name of the department project office or laboratory sponsoring the research and development. Include the address.)

Defence Research Establishment Ottawa, 3701 Carling Ave., Ottawa, Ontario, K1A 0Z4

9a. PROJECT OR GRANT NO. (if appropriate, the applicable research and development project or grant number under which the document was written. Please specify whether project or grant)

011LA

9b. CONTRACT NO. (if appropriate, the applicable number under which the document was written)

10a. ORIGINATOR'S DOCUMENT NUMBER (the official document number by which the document is identified by the originating activity. This number must be unique to this document.)

DREO REPORT 1103

10b. OTHER DOCUMENT NOS. (Any other numbers which may be assigned this document either by the originator or by the sponsor)

11. DOCUMENT AVAILABILITY (any limitations on further dissemination of the document, other than those imposed by security classification)

(X) Unlimited distribution
( ) Distribution limited to defence departments and defence contractors; further distribution only as approved
( ) Distribution limited to defence departments and Canadian defence contractors; further distribution only as approved
( ) Distribution limited to government departments and agencies; further distribution only as approved
( ) Distribution limited to defence departments; further distribution only as approved
( ) Other (please specify):

12. DOCUMENT ANNOUNCEMENT (any limitation to the bibliographic announcement of this document. This will normally correspond to the Document Availabilty (11). However, where further distribution (beyond the audience specified in 11) is possible, a wider announcement audience may be selected.)

UNCLASSIFIED

SECURITY CLASSIFICATION OF FORM

13. ABSTRACT (a brief and factual summary of the document. It may also appear elsewhere in the body of the document itself. It is highly desirable that the abstract of classified documents be unclassified. Each paragraph of the abstract shall begin with an indication of the security classification of the information in the paragraph (unless the document itself is unclassified) represented as (S), (C), or (U). It is not necessary to include here abstracts in both offical languages unless the text is bilingual).

(U) Accurate radar tracking of targets flying at low altitudes above a smooth surface is difficult because of the surface reflection. We propose a solution based on deterministic physical modelling of the specular multipath and the maximum likelihood method. This report describes the techniques and the results of performance studies. We derive the Cramer-Rao bound and show the benefit of using the refined propagation model. Monte-Carlo simulations are employed to compare the performance with the Cramer-Rao bound and demonstrate threshold effects on target height estimation. Finally we present the results obtained with two X-band radar experimental systems. (U)

14. KEYWORDS, DESCRIPTORS or IDENTIFIERS (technically meaningful terms or short phrases that characterize a document and could be helpful in cataloguing the document. They should be selected so that no security classification is required. Identifiers, such as equipment model designation, trade name, military project code name, geographic location may also be included. If possible keywords should be selected from a published thesaurus. e.g. Thesaurus of Engineering and Scientific Terms (TEST) and that thesaurus-identified. If it is not possible to select indexing terms which are Unclassified, the classification of each should be indicated as with the title.)

Radar
Signal Processing
Propagation
Low-Angle Tracking
Maximum Likelihood
Cramer-Rao Bound

Y1

FEB 17 1992

NO. OF COPIES NOMBRE DE COPIES	COPY NO. COPIE N°	INFORMATION SCIENTIST'S INITIALS INITIALES DE L'AGENT D'INFORMATION SCIENTIFIQUE
1	1	DAG
AQUISITION ROUTE FOURNI PAR ▶	DREO	
DATE ▶	31 JANUARY 1992	
DSIS ACCESSION NO. NUMÉRO DSIS ▶	92-00838	

DND 1158 (6-87)

National Defence / Défense nationale

PLEASE RETURN THIS DOCUMENT TO THE FOLLOWING ADDRESS:

DIRECTOR
SCIENTIFIC INFORMATION SERVICES
NATIONAL DEFENCE
HEADQUARTERS
OTTAWA, ONT. - CANADA K1A 0K2

PRIÈRE DE RETOURNER CE DOCUMENT À L'ADRESSE SUIVANTE:

DIRECTEUR
SERVICES D'INFORMATION SCIENTIFIQUES
QUARTIER GÉNÉRAL
DE LA DÉFENSE NATIONALE
OTTAWA, ONT. - CANADA K1A 0K2

~~#103732~~

#103732